Degradation Analysis of Exciplex-Based Organic Light-Emitting Devices Using Carbazole-Based Materials

Houssein El Housseiny, Suzanne Fery-Forgues, Marc Ternisien, David Buso, Georges Zissis, Cédric Renaud

Degradation analysis of exciplex-based organic light-emitting devices using carbazole-based materials

Houssein El Housseiny[1], *Suzanne Fery-Forgues*[2], *Marc Ternisien*[1], *David Buso*[1], *Georges Zissis*[1] *and Cédric Renaud*[1,*]

[1] LAPLACE, CNRS, Université de Toulouse, UPS, INPT, 118 route de Narbonne, 31062 Toulouse cedex 9, France

[2]SPCMIB, CNRS UMR 5068, Université de Toulouse III Paul Sabatier, 118 route de Narbonne, 31062 Toulouse cedex 9, France

KEYWORDS: carbazole-based devices, degradation, aggregation-induced emission, electroplex, electromer, exciplex, traps, deep blue.

ABSTRACT

A spectral shift and new emission bands in the green and red regions have been observed in deep blue exciplex-based OLEDs using carbazole-based materials, namely Tris(4-carbazoyl-9-ylphenyl)amine (TCTA). To deeply understand the origin of these new bands, single-layer and bilayer TCTA-based OLEDs subjected to electrical and optical (UV) stresses were investigated using various optical, electrical, morphological, and chemical measurements. The results showed

that the stress-induced emission bands primarily originate from morphological changes rather than chemical changes. The accumulation of excitons in the TCTA layer induces molecular aggregation, leading to the formation of electrically-active electronic states, namely electroplexes and electromers, which lead to the appearance of additional emission bands in green and red regions. Impedance spectroscopy measurements on single-layer OLEDs complemented this study. The results showed that TCTA degradation affects charge injection and transport. It was concluded that the stress-induced emission bands are caused by aggregate-domain formation and are closely linked to the formation of electrically-active defects, which act as trap states for charge carriers in the TCTA bandgap.

1. INTRODUCTION

Because of their high efficiency, organic light emitting diodes (OLEDs) could be ideal components for future lighting systems[1]. They are particularly well adapted to panel systems that combine great flexibility, compactness and high resolution images[2–4]. OLEDs are currently solidifying their presence in mobile displays and televisions markets[5–8]. The color-stable deep blue emission of organic devices is still relatively difficult to achieve due to the high energy of excitons leading to highest energy dissipation, reducing device efficiency and affecting their color purity. Blue device degradation is the principal issue to overcome in the development of the next generation organic display technology[9]. During the two last decades, phosphorescent and thermally activated delayed fluorescent (TADF) OLEDs have been extensively studied due to their ability to achieve internal quantum efficiencies (IQE) of up to 100%. This high efficiency is attributed to the contribution of both singlet and triplet excitons to light emission. By comparison, conventional fluorescent OLEDs, which are based on the emission from singlet excitons, are limited to an IQE of 25% according to spin statistics rule[10–12]. However,

phosphorescent and TADF OLEDs consistently face issues with concentration quenching. This problem is closely linked to the relatively long lifetimes of excited triplet states, which lead to triplet-triplet annihilation (TTA), singlet-triplet annihilation (STA), and triplet-polaron quenching (TPQ)[13,14]. To limit this quenching effect, a host-guest strategy is typically employed, that consists in dispersing the emitter into host materials. For efficient energy transfer from host to guest in these systems, the host material has to possess a triplet energy level higher than that of the guest. Therefore, host materials with relatively large bandgap are typically required for the activation of phosphorescent and TADF luminophores[15]. Due to their high triplet energy levels (approximately 2.7-3.3 eV), carbazole-based materials are frequently employed as host materials in these devices[16]. Among these, carbazole derivatives such as Tris(4-carbazoyl-9-ylphenyl)amine (TCTA) are widely used in OLEDs as hole transport layers (HTL) and host materials. Despite the considerable progress made over the past three decades in developing high-performance OLEDs, the electroluminescent (EL) stability of OLEDs using large bandgap materials like TCTA remains substantially lower than those using narrower bandgap materials[17,18].

Carbazole derivatives, chemically related to aromatic amines, are commonly used in OLED materials. Their degradation behavior has been extensively studied since 2006. Previous research indicates that carbazole radical cations tend to dimerize, forming 3,3′-biscarbazole in solution[19,20]. This is further confirmed by cyclic voltammetry measurements, which show irreversible oxidation at position 3 of the carbazole unit[21]. Studies of TCTA-based OLED structures or films exposed to UV light have identified a dissociative reaction involving the central amine moiety[22]. This observation indicates that the initial dissociative step likely occurs through electronically excited molecules, a phenomenon that might significantly contribute to

device EL degradation. Wang *et al.*[23] have shown that positive polaron-exciton interactions can induce aggregation of a carbazole-based molecule (*i.e*. 4,4′-Bis(*N*-carbazolyl)-1,1′-biphenyl labeled CBP), leading to alteration of EL spectra. Indeed, energy transfer between a positive polaron and an exciton leads to the formation of an energetically unstable excited positive polaron. To reach a more stable energy state, intermolecular interactions occur, resulting in the formation of molecular aggregates. Furthermore, these authors observed that the mechanism of aggregation induced by polaron-exciton interactions is more pronounced above a bandgap threshold E_g of approximately 3.1 eV. Below this value, the aggregation of materials is a long-time process, whereas above E_g, aggregation occurs rapidly and significantly. In aggregate form, the molecules exhibit a smaller bandgap. Thus, the spectral red-shift and the appearance of new emission bands upon aging are likely the result of molecular aggregation processes. Furthermore, these aggregates can act as traps for charge carriers and promote non-radiative pathway via Aggregation Caused Quenching (ACQ), leading to a decrease in the efficiency of OLEDs. Yu *et al.*[24] showed that the long-wavelength bands observed in the emission spectra of CBP are caused by molecular aggregation, induced by excitons. They also demonstrated that a complexation between the aggregates and the ETL material takes place, which affects the position of this band and consequently influences the spectral shifts observed.

The origin of these new bands and the associated decrease in OLED efficiency remains uncertain. Notably, the spectral shift and appearance of new bands can potentially originate from various intermolecular species (complex states), including exciplexes, excimers, electroplexes and electromers[25–29]. Exciplexes and electroplexes emission is due to the relaxation of excited states of bimolecular complexes formed by different types of molecules. In contrast, emission from excimers and electromers results from the relaxation of excited states of bimolecular

complexes composed of identical molecules. Typically, emission from exciplex and excimer is observable in both photoluminescence (PL) and electroluminescence (EL) spectra while electroplex and electromer emission is observable only in EL, as it involves charged species that form exclusively under electrical bias.

The aim of this study is to discuss and identify the physical and chemical mechanisms responsible for spectral shifts and the emergence of new emission bands in TCTA-based OLEDs. To this purpose, bilayer and monolayer TCTA-based OLEDs were fabricated and investigated. OLED characteristics were analyzed under electrical and optical (UV light) stresses. Optical and electrical characteristics were measured and compared before and after degradation. The results show that the formation of excitons in the TCTA layer induces the formation of molecular aggregates, which can cause the creation of electronically active levels (electroplex and/or electromer) responsible for the degradation of TCTA-based OLEDs. The paper is organized as follows: we first describe the experimental frameworks used to characterize and to evaluate the optical, electrical and morphological properties of TCTA based devices. Then, we investigate TCTA based OLED characteristics upon optical and electrical stresses. The study is completed by morphology surface measurement and chemical analysis, which are carried out on TCTA thin film in order to correlate the origin of stress-induced emission band with a likely chemical degradation and/or aggregate–domain formation. Then, a solution is proposed to stabilize TCTA properties and the influence of electron transport layer on stress-induced emission is studied. Afterward, electrical features of TCTA thin film are investigated by impedance spectroscopy. Finally, the origin of stress-induced emission bands is discussed in relation within aggregate-induced emission and electrically activated defects.

2. EXPERIMENTAL SECTION

All devices were fabricated on 100 nm of Indium tin oxide (ITO) coated glass substrates from Kintec with a sheet resistivity 15Ω/square used as the anode. The ITO glass substrates were cleaned sequentially with deionized water, acetone, ethanol, isopropanol and treated with UV ozone right before organic deposition. In this work we use Tris(4-carbazoyl-9-ylphenyl)amine (TCTA) as hole transporting layer (HTL), 2,9-Dimethyl-4,7-diphenyl-1,10-phenanthroline (BCP), 2,2',2''-(1,3,5-Benzinetriyl)-tris(1-phenyl-1-*H*-benzimidazole) (TPBi) and 4,7-Diphenyl-1,10-phenanthroline (BPhen) as electron transport layers (ETL) and calcium Ca (99.99% from Sigma Aldrich) (80 nm) as cathode. The organic materials and the cathode were deposited by thermal evaporation in a multiple-source chamber under high vacuum ($<10^{-5}$ mbar). All the thickness were monitored by an *in situ* quartz crystal microbalance (QCM). Characterizations of the OLEDs were obtained under inert atmosphere. Electrical characterization (I-V) of devices was performed using a Current-Voltage source (Keithley). The electroluminescence and the photoluminescence spectra were measured by using a spectroradiometer (JETI SpecBos 1201). For ultraviolet (UV) irradiation, a lamp illuminating at 365 nm with a power density of 2.1 mW/cm^2 was used. Fourier Transform InfraRed (FTIR) spectroscopy was performed by a Bruker Vertex 70 spectrometer. The surface morphology was probed by Atomic Force Microscopy (AFM Bruker Multimode 8) in tapping mode. Impedance spectroscopy measurements were performed with a Solartron impedance analyzer.

3. RESULTS AND DISCUSSION

A- Evolution of OLED characteristics upon optical and electrical stresses

Figure 1 shows the EL spectra of OLED devices (ITO/TCTA (95 nm) /BCP (35 nm) /Ca (80 nm)) for various bias currents (ranging from 1 mA to 60 mA). For low driving current (below 15

mA), OLED displayed deep blue emission centered at 425 nm. TCTA and BCP displayed emission band at 390 nm[30] and 396 nm[31] respectively. This emission is attributed to the formation of emissive complexes such as exciplexes at TCTA/BCP interface, and it can be observed under both electrical (electroluminescence) and optical (photoluminescence) excitation (see Supplementary Figure S2)[32]. For bias currents exceeding 15 mA, an enlargement of the EL spectrum and the appearance of new emission bands in the green (~516 nm) and red (~640 nm) were clearly observed. Following the series of measurements conducted at different bias currents, a new EL measurement was performed for a bias current below 15 mA. The EL spectrum still showed the presence of both green and red emission bands. Therefore, the modification of EL spectra under the influence of the bias current is related to irreversible mechanisms. According to Kondakov *et al.*[33], the photodegradation of carbazole-based molecules such as TCTA results in bond breakages, leading to a change in emission wavelengths and a progressive decrease in efficiency. According to Wang *et al.*[23], the appearance of these new emission bands is likely due to the molecular aggregation of carbazole-based materials.

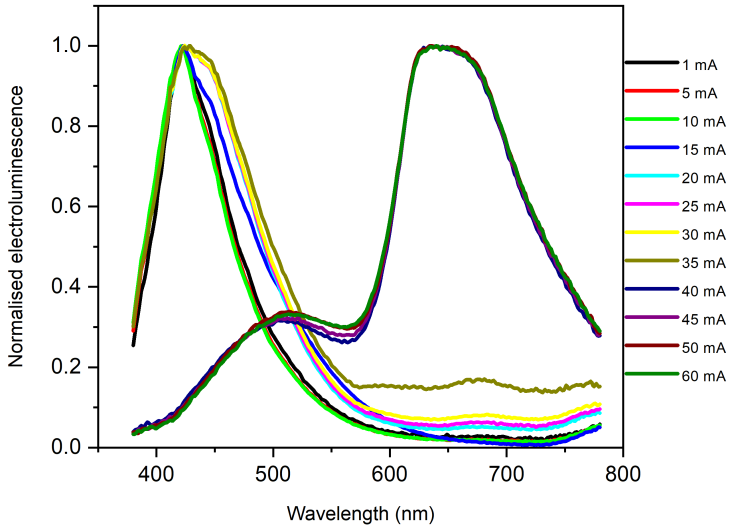

Figure 1. Normalized electroluminescence spectra of TCTA/BCP OLEDs for different driving currents measured between 1 mA and 60 mA

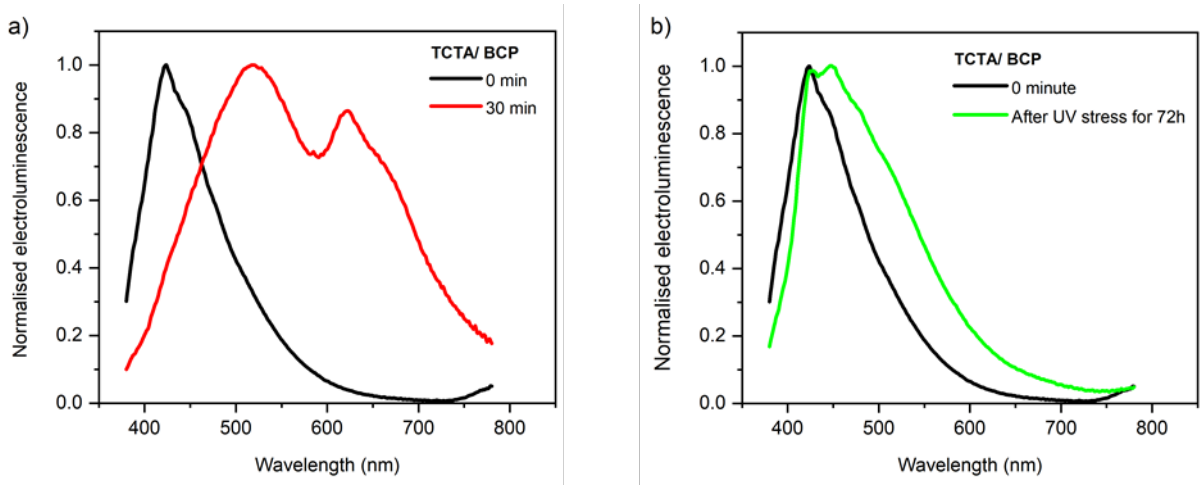

Figure 2. Comparison of normalized electroluminescence (EL) spectra of fresh-OLEDs (black curves) with stressed-OLEDs: **(a)** after electrical driving at 15 mA for 30 min, **(b)** after UV irradiation for 72 h

Excitons and polarons are the electronic species created during electrical stress. To determine which of these species is responsible for the appearance of new bands, we measured the EL spectrum of a sample irradiated by a UV lamp (λ_{em} = 365 nm) for 72 hours. Upon optical stress, only excitons are present within active layers. One of the samples was polarized at a constant current of 15 mA for a period of 30 min without UV irradiation (in dark condition). **Figure 2a&b** show the normalized electroluminescence (EL) spectra of the devices before and after electrical and UV stresses. The initial spectrum measured on fresh devices exhibited an emission at 423 nm, which was attributed to exciplexes formed between TCTA and BCP[32]. The EL spectrum of the same device was measured after electrical stress. As shown in **Figure 2a**, a red

shift occurred. Furthermore, it was observed that the blue emission peak vanished and two new bands at 526 and 621 nm clearly appeared. The EL spectrum measured after optical stress displayed a red shift with a peak centered at 449 nm. These results suggest that accumulation of exciton within active layers might be responsible for this spectral change.

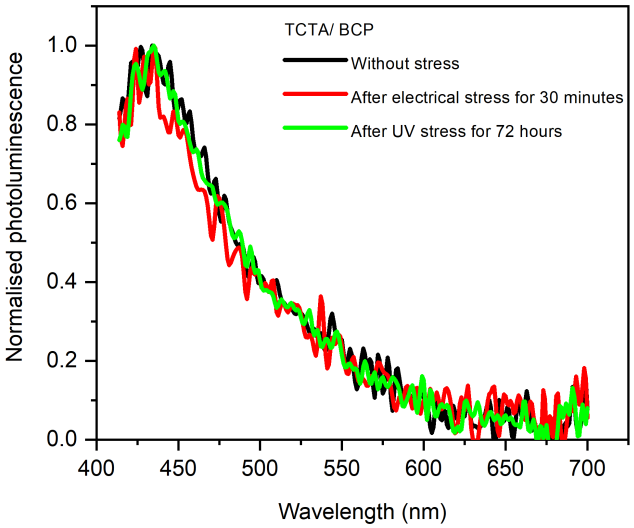

Figure 3. Normalized photoluminescence (PL) spectra of fresh-OLEDs (black curve) and stressed-OLEDs: after electrical driving at 15 mA for 30 min (red curve) and after UV irradiation for 72 h (green curve).

Figure 3 shows the PL spectra of the OLEDs after electrical and UV stresses. An emission band centered at 428 nm was observed. Neither UV stress nor electrical stress altered the PL spectra, which exhibited blue emission from exciplexes. A comparison of the electroluminescence (EL) and photoluminescence (PL) spectra of TCTA/BCP OLEDs after 72 hours of UV irradiation and electrical stress is provided in Supplementary Figure S3. Emission bands at 526 nm and 621 nm were observed only under electrical excitation (electroluminescence). Therefore, it can be concluded that these states are electrically activated and can thus be identified as electroplexes and/or electromers.

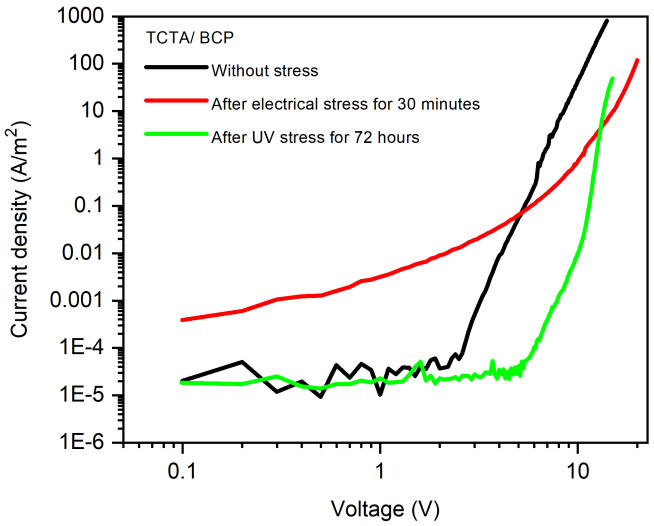

182

183 **Figure 4.** J-V characteristics in double logarithmic scale of TCTA/BCP OLEDs before and after
184 electrical and UV stresses

185 **Figure 4** displays the J-V characteristics measured before and after stresses (electrical and
186 optical). The threshold voltages ($V_{threshold}$) were evaluated at 5.6 V and 5 V after electrical and
187 UV stresses, respectively ($V_{threshold}$ = 2.5 V before stress). Upon the stress (electrical or optical),
188 we can note the following observations:

189 i) An increase in leakage current (for $V < V_{threshold}$) after electrical stress.
190 ii) An increase in the threshold voltage.
191 iii) A decrease in current density for $V > V_{threshold}$.

192 The increase in leakage current after electrical stress indicates the formation of a conduction path
193 between the electrodes, which could be due to the diffusion of chemical species from the
194 electrodes into the organic layers and/or the formation of defects likely associated with a
195 modification of the morphology of the organic layers (i.e. formation of aggregates)[34–37].

196 The increase in threshold voltage and the decrease in current after stresses (electrical or UV)
197 suggest a modification of the conduction properties of the organic layers. The change in the
198 characteristic shape under the influence of the electric field has been previously observed by Arif
199 *et al*. in polyfluorene-based diodes[38,39]. They attributed this change in J-V characteristics to the
200 formation of new trap states within bandgap of active layers.

201 The decrease in current density for voltages above $V_{threshold}$ after degradation could be explained
202 by the decrease in the mobility of injected charges and/or by an increase in electrically-active
203 defects (traps). This decrease also confirms that the organic layers become more resistive after
204 degradation[40,41]. The formation of domains, which can act as trap for charge carriers, reduces the
205 efficiency of OLEDs. This could be linked to a modification of the morphology of the organic
206 layers (such as aggregate domain formations). These might lead to a decrease in current density
207 and a shift in the EL spectrum.

208 Moreover, the turn-on voltages V_{ON} (evaluated for a luminance of 1 cd/m²), was increased from
209 9.3 V for the fresh device to 12.5 V and 13 V after electrical and UV stresses, respectively.
210 Additionally, a decrease in luminance was observed after both electrical and optical stresses (see
211 Supplementary Table S1).

212 **B- Chemical analysis and morphology surface investigation of TCTA thin film**

213 **B1- Fourier Transform InfraRed Spectroscopy**

214 Carbazole derivatives are chemically related to aromatic amines. It has been demonstrated that
215 the degradation of aromatic amines is caused by their relatively weak carbon-nitrogen C-N bond,
216 which is close to the energy of the first excited singlet state S_1 for blue emitters, a phenomenon
217 that may significantly contribute to the device EL degradation[42]. Excitation can occur either
218 through the recombination of holes and electrons (formation of excitons by electrical excitation)

or even by UV light absorption. Since the S_1 energy of the blue emitter is greater than or comparable to the bond dissociation energy (BDE), bond cleavage is likely to occur. TCTA has a triangular molecular structure, with a triphenylamine core linked to three carbazole units forming this molecule (**Figure 5**). This results in two types of C-N bonds: three C (sp^2)-N (sp^3) bonds in the triphenylamine subunit and three C (sp^2)-N (sp^2) bonds between the phenyl groups and the carbazole groups. The neutral bond dissociation energies (BDE) of C (sp^2)-N (sp^3) and C (sp^2)-N (sp^2) calculated by Song and Lee[43] are 3.2 eV and 3.6 eV, respectively. The anionic BDE values for the same C (sp^2)-N (sp^3) and C (sp^2)-N (sp^2) bonds are 0.8 eV and 1 eV, respectively[43]. No voltages were applied to the TCTA film during this experiment, and hence the density of anionic states is very weak. Therefore, the BDE in neutral form was considered to explain the degradation under UV exposure. The energy of the first excited singlet state S_1 of TCTA, as reported in the literature, is 3.4 eV[44]. The bond dissociation energy of the C (sp^2)-N (sp^3) bond is lower than the energy of the first excited singlet state. The study of OLEDs containing TCTA exposed to UV light revealed homolytic cleavage of C (sp^2)-N (sp^3) bonds rather than C (sp^2)-N (sp^2) bonds[42,43]. This leads to non-radiative recombination and quenching processes, resulting in a loss of luminance efficiency. Thus, it is possible that the spectral shift observed in TCTA-based OLEDs is caused by species formed during the chemical decomposition of TCTA.

To determine the nature of the chemical bonds present and to check for any bond breakage due to UV light, FTIR (Fourier Transform InfraRed Spectroscopy) measurements were performed. **Figure 6** shows the FTIR spectra for 500 nm TCTA films (deposited on a silicon substrate) before and after UV irradiation for 92 hours. The peak at 3047 cm^{-1} is attributed to the C-H bond (*aromatic C-H stretching vibration*), those at 1599 cm^{-1}, 1508 cm^{-1}, and 1452 cm^{-1} correspond to the C=C bond (*aromatic C=C stretching vibration*), the bands at 1311 cm^{-1}, 1280 cm^{-1}, and 1230

242 cm^{-1} are attributed to the C-N bond (*amine C-N stretching vibration*), and finally, those between
243 675 and 900 cm^{-1} correspond to the C-H bond (*out of plane bending vibrations of aromatic*
244 *rings*). The results obtained have shown no change in the infrared (IR) spectra recorded before
245 and after UV degradation, particularly between 1230 cm^{-1} and 1311 cm^{-1}, the range
246 corresponding to the C-N bond, which is susceptible to break. Thus, the FTIR results suggest that
247 no chemical decomposition of TCTA occurred following UV irradiation. Additionally, mass
248 spectrometry and proton nuclear magnetic resonance (^{1}H NMR) spectroscopy measurements
249 were conducted on TCTA microcrystals before and after 72 hours of UV irradiation (see
250 Supporting Information). These measurements enable the detection of any products formed after
251 degradation, provide information on the chemical structure of unknown organic materials, and
252 allow to quantify their amounts. According to the results obtained, no difference was observed
253 between the initial and irradiated products, confirming the chemical stability of the compound.

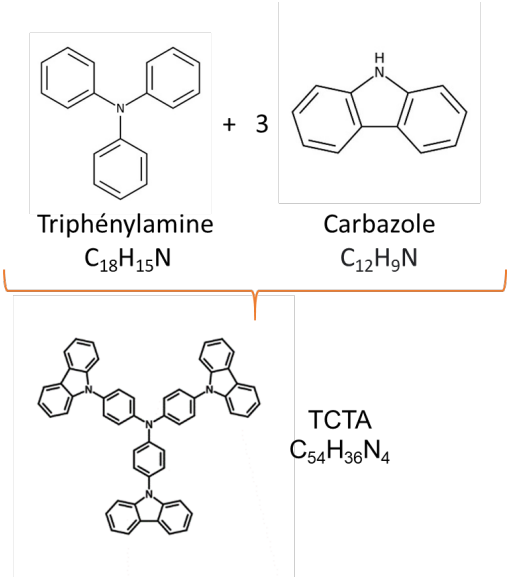

254

255 **Figure 5.** Molecular structures of Triphénylamine, Carbazole and TCTA

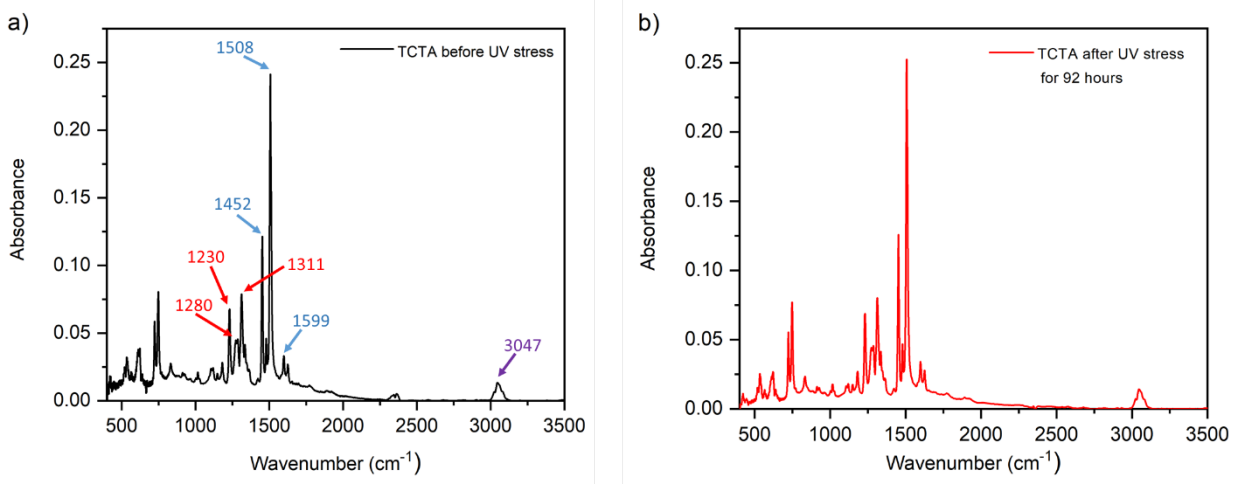

Figure 6. FTIR spectra of TCTA film collected **(a)** before and **(b)** after irradiation with UV light for 92 h

B2- Surface analysis by AFM

AFM measurements were performed to visualize the surface topography and to measure the roughness of the TCTA layers before and after degradation. This technique is commonly used to evaluate changes in morphology and roughness of organic materials during degradation. A 100 nm thin layer of TCTA deposited on a glass substrate was subjected to UV first for 48 hours and then for 72 hours (under nitrogen). **Figure 7** shows the AFM images and the Root Mean Square (R_{ms}) roughness of the irradiated and non-irradiated samples.

The R_{ms} roughness was 3.5 nm for the non-irradiated TCTA sample (**Figure 7a**). However, we observed a slight increase in roughness to 4 nm when the TCTA layer was exposed to UV light for 48 hours (**Figure 7b**). The same sample was then placed under UV light for an additional 24 hours. A second measurement was performed on the substrate, which has been irradiated for a cumulative duration of 72 hours. R_{ms} underwent a significant increase, reaching 14.8 nm (**Figure 7c**).

This confirms that exposure of the samples to UV light induces morphological changes on the surface of TCTA, affecting the roughness of the TCTA layer. Indeed, studies conducted by Liu *et al.*[45] and Li *et al.*[46] suggest that the increase in roughness is due to the formation of molecular aggregates following degradation. Additionally, the phase image (see Supplementary Figure S7) of pristine TCTA thin film did not show any significant change in contrast, indicating that the surface is uniform. After UV-stress (for 72h), a slight change in contrast was noticed. The roughness variation could be attributed to the formation of a new phase.

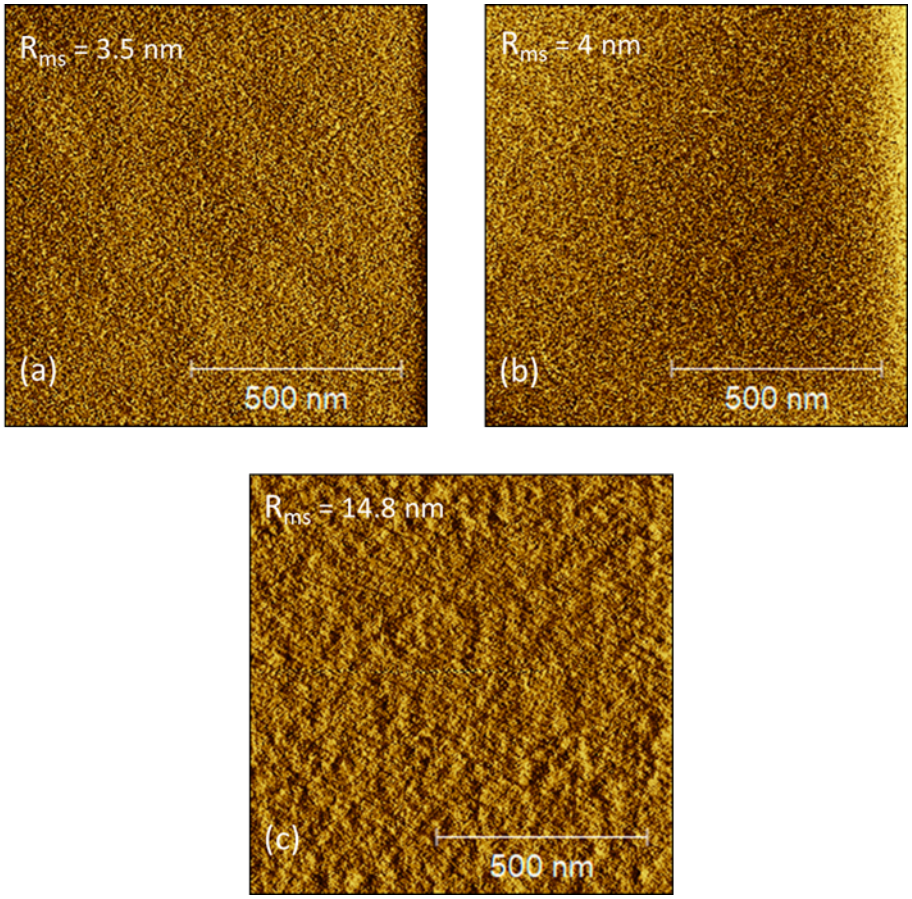

Figure 7. AFM surface scan and root mean square (R_{ms}) roughness of TCTA films: **(a)** non-irradiated, **(b)** UV-irradiated for 48 h and **(c)** UV-irradiated for 72 h

C- Stabilization of optical properties of TCTA thin film by using material mixing

To further verify that the spectral shift is due to intermolecular interactions of TCTA (aggregation of TCTA), the TCTA layer was mixed with BCP molecules. The doping ratio was set at 70 wt%. This percentage is sufficient for the BCP molecules to act as molecular "spacers" between the TCTA molecules, thereby limiting their aggregation.

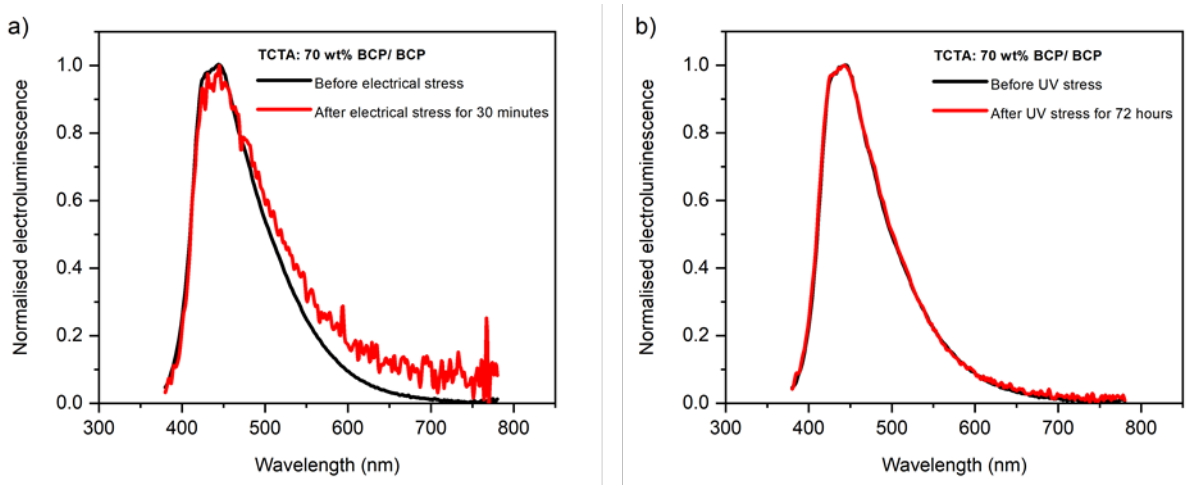

Figure 8. Normalized electroluminescence (EL) spectra of TCTA:70 wt% BCP OLEDs without stress and **(a)** after electrical driving at 15 mA for 30 min, **(b)** after UV-irradiation for 72 h

Figure 8a shows the electroluminescence spectra of the ITO/TCTA:70 wt% BCP (95 nm) /BCP (35 nm)/ Ca (80 nm) structure collected before and after electrical driving at 15 mA for a period of 30 min, and **Figure 8b** shows the spectra before and after UV irradiation for 72 h OLEDs exhibited similar spectra before and after the stress tests (electrical or UV); no spectral shift or appearance of new bands were noted. In this case, an emission band between 427 and 444 nm was observed, corresponding to exciplexes formed between TCTA and BCP. These results

indicate that the introduction of BCP into the TCTA layer tends to reduce the aggregation or dimerization of TCTA molecules. This observation further supports the conclusion that the spectral shift and the appearance of new emission bands in OLEDs after degradation are associated with intermolecular interactions between TCTA molecules (molecular aggregation of TCTA induced by excitons).

To better understand the nature of the species inducing this spectral shift and the potential role of ETL materials, we investigated the effect of ETL layer on emission wavelengths of electroluminescence spectra during electrical bias. For this purpose, the structure ITO/ TCTA (95 nm) /ETL (35 nm) /Ca (80 nm) was fabricated to study structures with the same HTL material but three different ETL materials.

D- Influence of ETL on stability of TCTA-based OLEDs

BCP, TPBi, and Bphen are the three ETL materials used in this study. The devices were electrically biased at 15 mA for a period of 30 minutes. Their electroluminescence (EL) spectra were measured periodically, every minute for 30 min. The normalized EL spectra of the three structures are depicted in **Figure 9**.

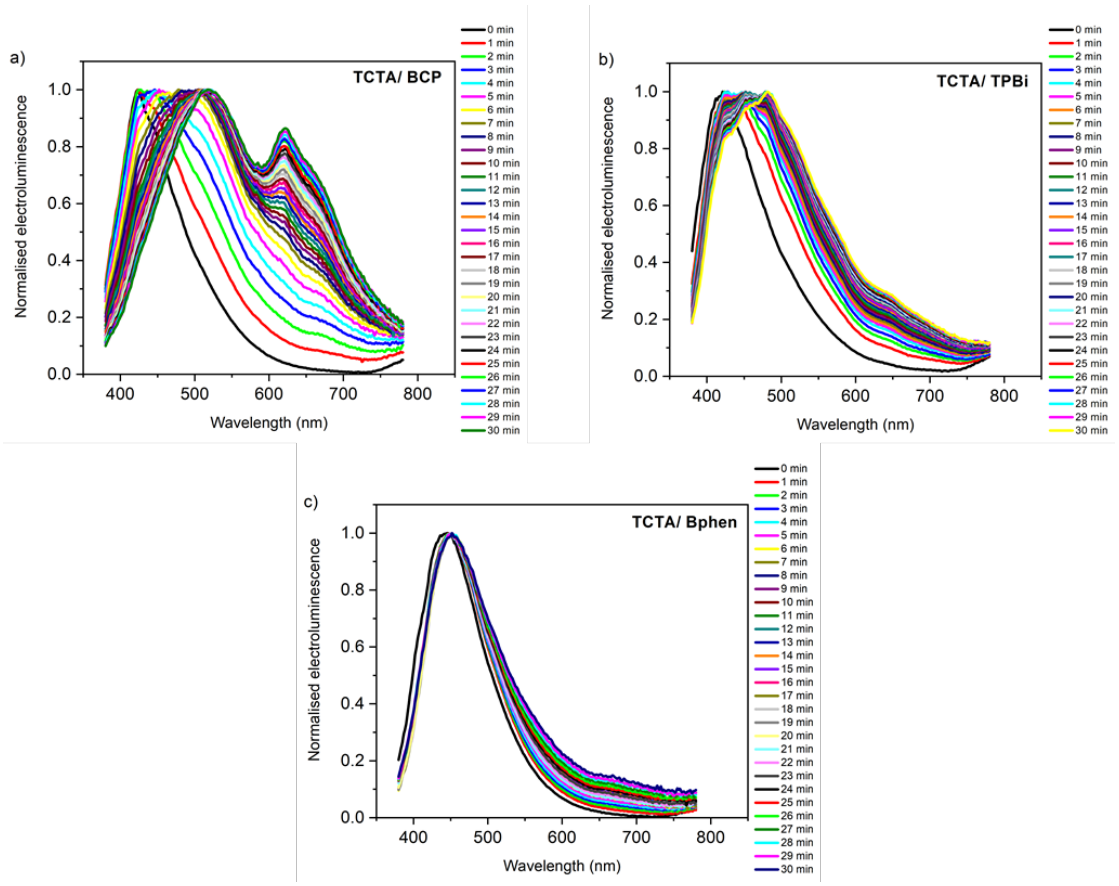

Figure 9. Normalized electroluminescence (EL) spectra of TCTA/ETL OLEDs with **(a).** BCP, **(b).** TPBi, and **(c).** Bphen used as the ETL materials, collected after electrical driving at 15 mA, measured every minute for 30 min

The initial spectra of the devices with BCP, TPBi, and Bphen materials exhibited emissions at 423, 418, and 444 nm, respectively, corresponding to exciplexes formed between TCTA and ETL layer[32], [47], [48]. For the structure with BCP, we observed the emergence of two new bands with peaks at 526 and 621 nm that evolved over time, while the blue peak at 423 nm tended to disappear. For the device with TPBi, a red-shift of the spectrum, the appearance of a broad band peaking at 482 nm and a weak emission at 645 nm were noted. For the structure with Bphen, a new band with a maximum at 452 nm and a weak emission at 661 nm were observed. Based on

these results, it was concluded that the wavelengths of the new bands depend on the nature of the ETL layer. This suggests that the appearance of these new bands may originate from specific species involving both TCTA and ETL. Indeed, studies have shown that aggregates of carbazole-based molecules, formed after degradation, interact with molecules in the ETL layer to generate complex species responsible for these new bands[49]. The geometry of the ETL material molecules and the intermolecular separation between TCTA and ETL play an important role in this shift[24]. Over time, the intensity of these new peaks increases, attributed to a rise in the density of these complexes[50]. Indeed, the molecular reorientation and reorganization necessary for aggregate formation exhibit relatively slow formation times (on the order of a few seconds)[51].

A similar study was performed on an OLED by replacing the TCTA layer with an NPD layer. The OLEDs have the following structure: ITO/ NPD (95 nm)/ TPBi (35 nm)/ Ca (80 nm). The OLEDs are electrically driven at 15 mA for a period of 30 minutes. As in the previous study, the EL spectra were collected every minute.

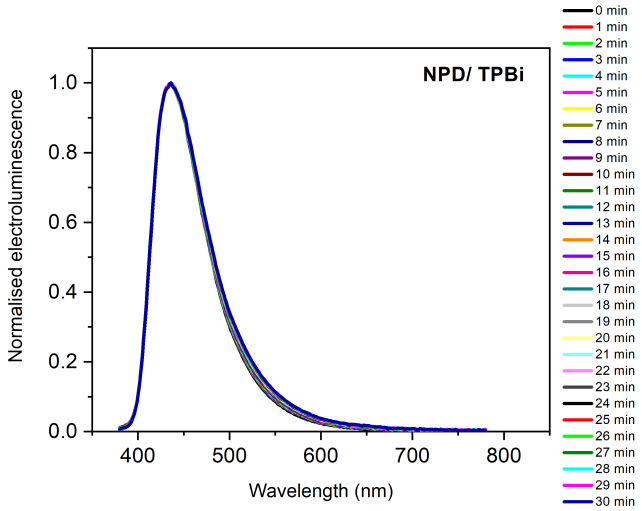

Figure 10. Normalized electroluminescence (EL) spectra of NPD/TPBi collected after electrical driving at 15 mA, measured every minute for 30 min

As shown in **Figure 10**, there were no significant changes in the EL spectra over time. The spectra exhibited one peak centered at 435 nm, corresponding to the emission of NPD, and no new bands were detected after electrical stress. Therefore, the modification of the EL spectrum after degradation is specific to TCTA-based OLEDs.

E- Investigation of TCTA monolayer based devices

In order to deeply understand the origin of these new bands, measurements of electroluminescence spectra (EL), J-V characteristics and impedance spectroscopy (IS) were performed on single-layer OLEDs without ETL, with the structure ITO/TCTA (100 nm)/Ca (80 nm). These measurements were performed on unstressed devices immediately after fabrication and on devices exposed to a UV source (λ_{em} = 365 nm) for 72 h UV irradiation induces the $S_0 \rightarrow S_1$ transition, leading to the formation of singlet excitons similar to those produced during electrical bias.

E1- Optical and electrical characteristics

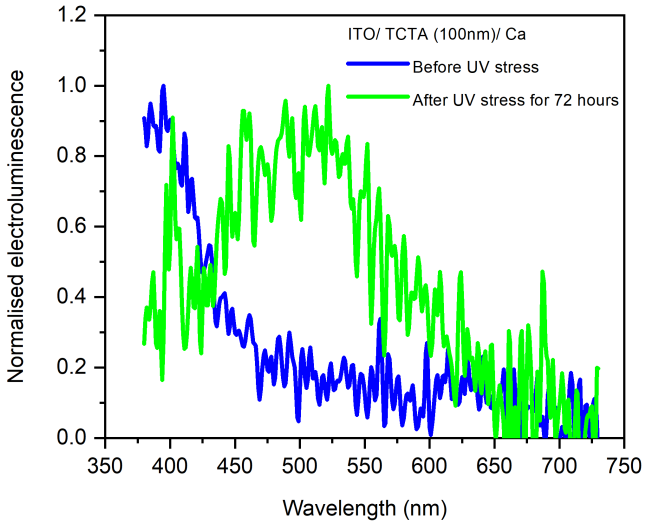

Figure 11. Normalized electroluminescence spectra of TCTA monolayer based fresh device (blue curve) and after irradiation with a UV source for 72 h (green curve)

Figure 11 shows the normalized electroluminescence spectra of a single-layer OLED based on TCTA immediately after fabrication (blue curve) and after UV irradiation for 72 h (green curve). The fresh device showed an emission at 390 nm, which corresponds to the emission of TCTA in a thin film. After optical stress, the EL spectrum exhibited a red-shift. The OLED displayed an emission in the green region centered around 510 nm. A peak at 400 nm also seemed to be present, which corresponds to the emission band of the TCTA monomer. Measurements of the EL spectra after degradation at various current density values did not show UV emission (at 390 nm), but only green emission. It is noteworthy that this spectral shift was observed exclusively in electroluminescence. The samples exhibited a similar PL spectrum before and after optical stress, indicating that the green emission band is electrically activated and arises from electromers. The formation of excitons under optical stress appears to induce the creation of electromers in the TCTA layer, which display a green emission band. It is consistent with the formation of the green emission bands observed in multilayer TCTA/BCP OLEDs. These bands originate from electromers that form in the TCTA layer after electrical or optical stress. The presence of excitons seems to play a key role in the formation of electromers within the TCTA layer. Unlike multilayer structures, the red emission band (at 621 nm) was not observed in single-layer OLEDs. This suggests that this emission band is strongly associated with the formation of an electronic state at the TCTA/BCP interface. Furthermore, since this emission band has been identified as electrically activated, we can conclude that it is related to the formation of an electroplex state at the TCTA/BCP interface.

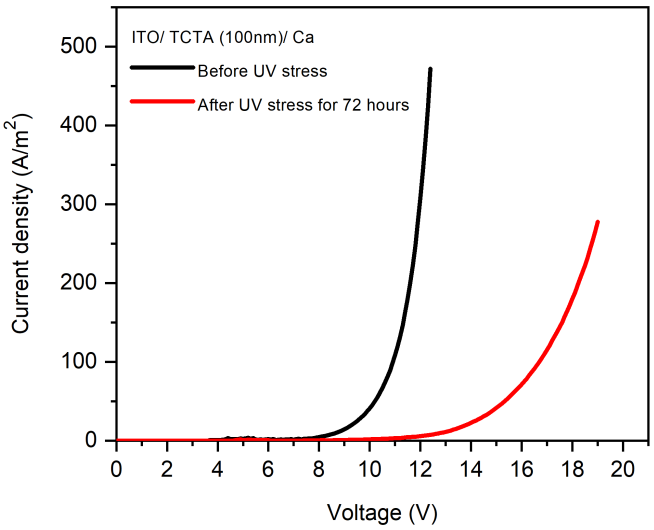

Figure 12. J-V characteristics of TCTA organic layer based fresh device (black curve) and after UV-irradiation for 72 h (red curve)

We measured the current density versus voltage (J-V characteristics) for the OLEDs before and after UV degradation. As shown in **Figure 12**, the J-V curve shifted towards higher voltages after degradation. After UV stress, the current density of the OLED decreased, indicating a reduction in the conductivity of the TCTA layer[40,41 52].

E2- Impedance spectroscopy (IS)

To study the electrical properties, charge trapping and transport within the organic layers, impedance spectroscopy (IS) measurements were performed. These measurements involve applying a small sinusoidal signal $V_{AC}(t) = V_m \sin(2\pi f.t)$, where V_m is the amplitude and f is the frequency, superimposed on a DC voltage V_{DC}. The total applied voltage is $V = V_{DC} + V_m \sin(2\pi f.t)$. Using this technique, we can measure the impedance $|Z|$ as a function of frequency f, the capacitance C as a function of voltage, and the equivalent circuit parameters of the OLED. These

parameters provide information about the accumulated charges (traps) in the organic layer and the injection behavior at various interfaces.

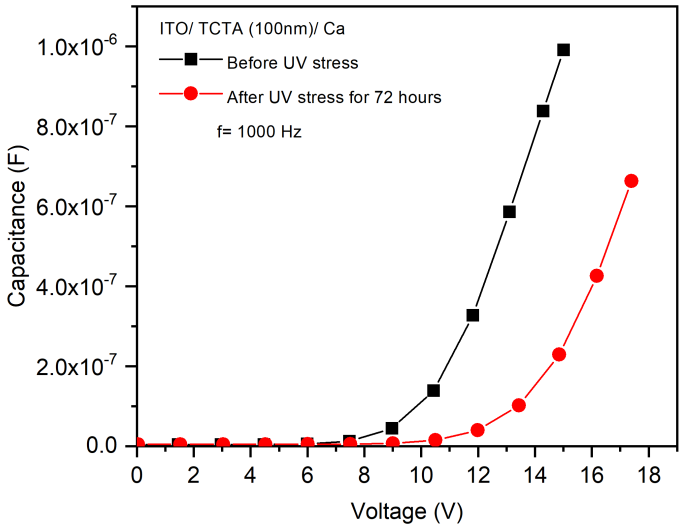

Figure 13. C-V characteristics of single TCTA based fresh OLEDs (black curve) and after UV-irradiation for 72 h (red curve) measured at 1000 Hz

C-V Measurements were performed on single-layer OLEDs based on TCTA, both non-degraded and UV-stressed. The C-V curves obtained at a frequency of 1 kHz are shown in **Figure 13**. For voltages below 6 V for TCTA (unstressed) and 7.5 V for TCTA (UV-stressed), the capacitance remained constant, indicating that no charges are injected into the TCTA layer. Charges accumulate at the electrode levels. This capacitance is the geometric capacitance (C_{geo}) of the OLED. It is independent of frequency and voltage and is given by the following relation:

$$C_{geo} = \frac{\epsilon_0 \epsilon_r S}{d} \quad (1)$$

where ϵ_0 is the permittivity of free space, ϵ_r is the relative permittivity of the organic material, S is the surface area of the organic substrate, and d is the thickness of the organic layer.

From 6 V for unstressed TCTA and 7.5 V after UV-stress, the external field compensates for the internal field of the OLED. Consequently, charges begin to be injected and accumulate in the organic layer. The distance between the two charged regions is thus reduced, and a diffusion capacitance C_{diff} is added to the geometric capacitance, resulting in an increase in capacitance with increasing voltage. The total capacitance of the diode is then given by: $C_{Totale} = C_{géo} + C_{diff}$. After degradation, we observed a decrease in the total capacitance. C_{geo} remained unchanged after degradation. Indeed, the surface area and thickness of the active layer did not change after UV stress. The variation in total capacitance is attributed to the decrease in diffusion capacitance. The transition voltage V_{tr}, where the capacitance begins to increase, depends on the built in voltage of the OLED (theoretically given by the difference between the work functions of the electrodes: $V_{bi} = W_{ITO} - W_{Ca}$) and the presence of a local electric field at the interfaces between the organic layer and the electrodes. V_{tr} is given by[53–55] :

$$V_{tr} = \frac{Q}{\epsilon_0 \epsilon_r} d + V_{bi} \qquad (2)$$

Q is the charge density present at the interface between two materials (for example, the organic layer and one of the two electrodes).

A V_{tr} voltage greater than V_{bi} indicates a positive charge. The V_{tr} voltage is 6 V for fresh OLED and 7.5 V for degraded OLED. Both OLEDs have the same structure, thus they have the same V_{bi} and geometry (thickness and surface area). Therefore, an increase in the V_{tr} voltage suggests that UV stress leads to an increase in the density of fixed positive charges present at one of the two interfaces, either ITO/TCTA or TCTA/Ca. The interfacial charge density was increased by

0.4 $mC.m^{-2}$ due to the degradation of the TCTA layer. Several studies have reported an increase in the transition voltage V_{tr} due to the degradation of Alq_3 based OLEDs caused by the formation of unstable Alq_3^+ cations[53,56–58]. Kondakov *et al.* also demonstrated that degradation under irradiation of certain hole transport layers leads to the formation of fixed positive charges acting as hole traps[52].

Impedance spectroscopy measurements also allow us to plot the impedance |Z| as a function of frequency *f* before and after degradation. To deeply understand and interpret the changes in the electrical behavior of OLEDs after degradation, we present the equivalent circuit of a single-layer OLED as described from the literature[59].

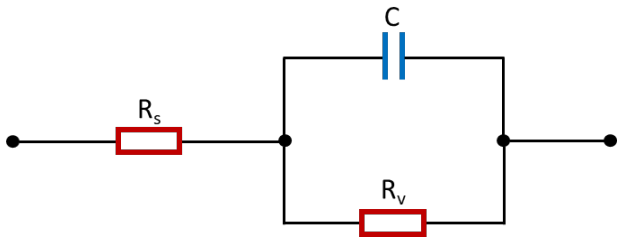

Figure 14. Equivalent circuit of a single-layer OLED

The equivalent circuit of a single-layer OLED (**Figure 14**) can be represented by a combination of ohmic resistances and a capacitor. This circuit includes the following elements:

R_s: The contact resistance, representing the resistance at the interface between the electrodes and the organic layer.

C: The bulk capacitance of the organic layer.

R_v: The bulk resistance, representing the resistance to charge transport within the organic layer.

The impedance of the equivalent circuit is given by:

$$Z = R_s + \frac{1}{\frac{1}{R_v} + j\omega C} \quad (3)$$

443 $$Z = \left[R_s + \frac{R_v}{1+(\omega\tau)^2}\right] - j\left[\frac{\omega\tau R_v}{1+(\omega\tau)^2}\right] = Z' - jZ'' \quad \text{avec} \quad \tau = R_v C$$

444 $$Z' = R_s + \frac{R_v}{1+(\omega\tau)^2} \quad \text{et} \quad Z'' = \frac{\omega\tau R_v}{1+(\omega\tau)^2}$$

445 The impedance amplitude of the equivalent circuit is: $|Z| = \sqrt{(Z')^2 + (Z'')^2}$

446 • For f= 0 Hz : $Z' = R_s + R_v$; $Z'' = 0$; $|Z| = R_s + R_v$

447 • For f= ∞ : $Z' = R_s$; $Z'' = 0$; $|Z| = R_s$

448 From equation 3, the relaxation frequency is defined as:

$$f_r = \frac{1}{2\pi R_v C} \quad (4)$$

449 The relaxation frequency can be related to the conduction properties of the organic layer. A
450 decrease in the conductivity of the organic layer leads to a shift towards lower frequencies. The
451 conductivity ($\sigma_v = \frac{L}{R_v S}$) in organic semiconductors is thermally activated and follows the
452 Arrhenius law, given by the following relation:

$$\sigma_v = \sigma_0 \exp(-\frac{E_a}{2.k.T}) \quad (5)$$

453 where σ_0 is the conductivity at 0 K, E_a is the activation energy, T is the temperature and K is the
454 Boltzmann constant.

455 The impedance |Z| as a function of frequency f (|Z| -f) in a range from 1 Hz à 10^5 Hz were
456 measured on TCTA OLEDs (fresh device) and TCTA OLEDs (UV-stressed) at a voltage of 9 V.

The results are shown in **Figure 15**. It can be clearly observed that the impedance increases after degradation and that the (|Z| -f) curve of the degraded OLED shows fluctuations. These fluctuations may be caused by a trapping/detrapping phenomena within the organic layer. The relaxation frequency was evaluated at 5275 Hz for the non-degraded OLED and 862 Hz for the degraded OLED. The decrease in relaxation frequency suggests that UV stress leads to an increase in the resistance of the TCTA layer (according to equation 4) and consequently a decrease in the conductivity of the TCTA layer. Charge transport becomes more dispersive upon ageing. According to equation 5, a decrease in conductivity is associated with an increase in activation energy. UV stress leads to the formation of electrically-active defects, which act as trap levels in the bandgap and thus reduce charge conduction in the TCTA layer. Nowy *et al.* have studied the degradation of OLEDs under electrical stress[53]. They have observed that after the degradation of the OLED, the relaxation frequency shifted to lower frequencies, indicating a decrease in charge mobility due to traps present within the volume of the organic layers. TCTA is a hole-transporting material, with holes being the majority carriers in the TCTA layer. The conduction observed through impedance spectroscopy can be attributed to holes. The electrically-active defects induced by UV stress are probably hole-like traps.

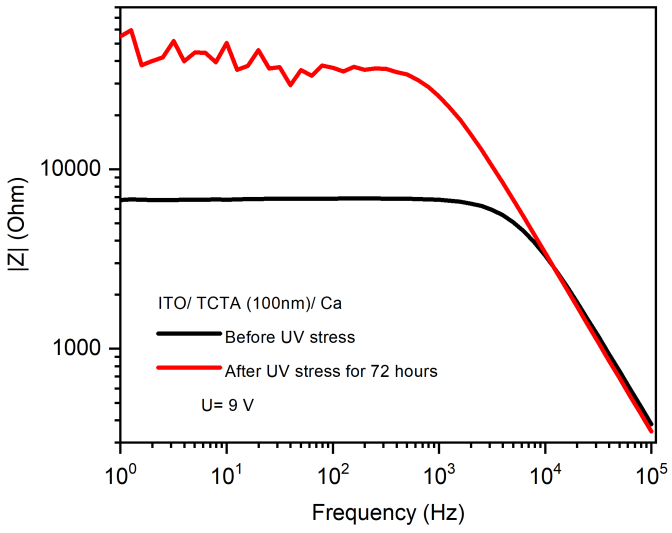

Figure 15. |Z|-f curve measured on single TCTA fresh OLEDs (black curve) and after UV degradation measured at 9 V (red curve)

Table 1. The values of resistances R_s and R_v of the equivalent circuit of fresh and UV-stressed TCTA-based OLEDs

Sample	R_s (Ohm)	R_v (Ohm)
TCTA (Unstressed)	68.295	6749.4
TCTA (UV-stressed)	334.28	39823

Based on the equivalent circuit of the single-layer OLED (**Figure 14**) and after modeling the |Z|-f curve, the contact resistance R_s and the bulk resistance R_v can be evaluated with a precision of +/- 3 Ohms (**Table 1**). A significant increase in the circuit resistances after degradation was observed. The increase in R_s is consistent with a limitation in charge injection into the organic layer, while the increase in R_v suggests a decrease in charge mobility within the TCTA layer.

F- Formation of defect-related emission band in TCTA-based OLEDs

Cho *et al.* observed the formation of electromers in carbazole-based organic layers associated with the development of morphological defects[60]. Kwon *et al.* demonstrated that the injection of electrons into a triphenylamine-based HTL (TAPC) layer induces the formation of electrically-active defects, leading to the formation of electromers[61]. These defects are associated with local morphological changes in the HTL layer, which lead to the formation of trap levels within the HTL layer's gap, thereby altering the layer's conduction properties. Thus, it can be hypothesized that the formation of electromers in the TCTA layer (after electrical and/or optical stress) is related to the creation of a trap level in the TCTA bandgap. Consequently, we attempt to estimate

494 the activation (E_a) energy of the trap level E_t.

495 The maximum emission energy of photon can be expressed as follows [62–66] :

$$h\nu_{exc} = I_P(D) - E_A(A) - E_C \quad (6)$$

496 where $I_P(D)$ is the ionization potential of the donor, $E_A(A)$ is the electron affinity of the acceptor
497 and E_C is the coulombic attraction energy that can be written:

$$E_C = \frac{e^2}{4\pi\varepsilon_0\varepsilon_r r_{D^+A^-}} \quad (7)$$

498 where e is the elementary charge (1.6×10^{-19} C), ϵ_0 is the dielectric permittivity ($8.85\times$
499 10^{-12} F. m^{-1}), ϵ_r is the relative dielectric constant of organic material (~3 for organic materials
500 used) and $r_{D^+A^-}$ is the electron-hole separation.

501 Assuming that the electromer responsible for the green emission is due to the presence of a trap
502 level located in the gap of TCTA, this must be considered in relation (6). The maximum photon
503 emission energy $h\nu_{exc}$ becomes:

$$h\nu_{exc} = I_P(D) - E_A(A) - E_C - E_a \quad (8)$$

504 Where $E_a$is the activation energy of the hole trap.

505 According to the literature, the minimum radius associated with an electromer is 0.7 nm[67]. Using
506 the ionization potential (I_P) and electron affinity (E_A) values of TCTA (**Table 2**), the minimum
507 activation energy of the hole trap E_a is estimated at approximately 1.1 eV for an emission at 510
508 nm (from electromer).

Table 2. The ionization potential of TCTA (donor), the electron affinity of BCP (acceptor), the maximum photon emission energy $h\nu_{exc}$ of TCTA/BCP and single TCTA organic layer devices, E_C the Coulombic attraction energy and the activation energy of the hole trap

Electromer: emission at 510 nm	I_P (TCTA) (eV)	E_A(TCTA) (eV)	$h\nu_{exc}$ (eV)	E_C (eV)	E_a (eV)
	5.80*	1.60**	2.42***	0.68	~ 1.1
Electroplex: emission at 621 nm	I_P (TCTA) (eV)	E_A(BCP) (eV)	$h\nu_{exc}$ (eV)	E_C (eV)	E_a (eV)
	5.80*	1.89**	2.00***	0.81	~ 1.1

* The ionization potential (I_P) determined by photoemission yield spectroscopy (PYS) and **the electron affinity E_A by low energy inverse photoemission spectroscopy (LEIPS)[68].***The energy $h\nu_{exc}$ evaluated from the emission peak of the EL spectrum

The red emission observed in OLEDs based on TCTA/BCP originates from electroplexes present at the TCTA/BCP interface. A calculation can be performed by considering that this hole trap E_t contributes to the electroplex emission. Using relation (8), we calculated the Coulombic attraction energy E_C, and from relation (7), we estimated the radius $r_{D^+A^-}$, which could provide an indication of the nature of the emission. According to the literature, the e-h separation distance of the electroplex is about 0.4-0.7 nm. In our case, we obtained a Coulomb capture radius of 0.59 nm, which is favorable for the formation of an electroplex. It can be assumed that the same trap level E_t (with E_a= 1.1 eV), attributed to hole-like traps, would contribute to the formation of an electroplex $|E_t^+A^-\rangle$ (red emission) and an electromer $|E_t^+D^-\rangle$ (green emission).

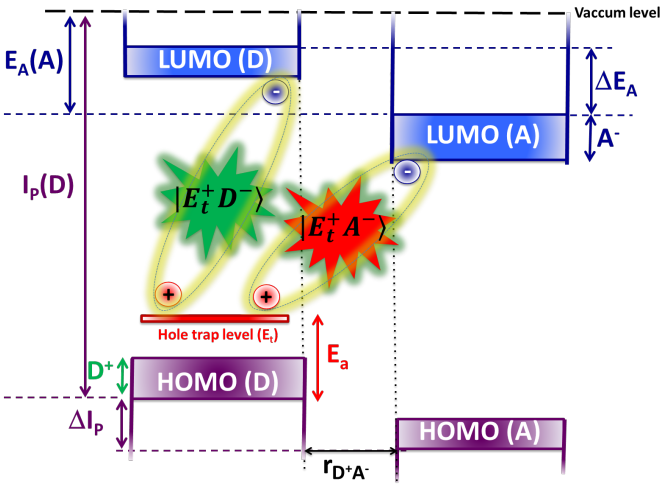

525

526 **Figure 16.** Formation mechanism of the electroplex $|E_t^+A^-\rangle$ and the electromer $|E_t^+D^-\rangle$

527 The formation process of electroplexes and electromers can be illustrated by **Figure 16**.
528 Thermally Stimulated Current (TSC) measurements and Deep-Level Transient Spectroscopy
529 (DLTS) characterizations, would allow to validate the activation energy of the traps and the
530 nature of these levels associated with the emission of the electromer and the electroplex[39,69].

531 ## 4. CONCLUSION

532 Complete studies conducted on single-layer and multilayer OLEDs based on TCTA have shown
533 a degradation of the EL spectrum after electrical and optical (UV) stress. After aging, a spectral
534 shift and the emergence of new emission bands in the green and red regions were observed.
535 These two emission bands are electrically activated. The green emission band is identified as an
536 electromer originating from the TCTA layer, while the red emission band is attributed to the
537 formation of an electroplex between the TCTA and the BCP layer. FTIR and chemical
538 measurements confirmed that the TCTA molecule does not undergo any bond cleavage after
539 degradation. AFM studies on irradiated TCTA films showed that UV stress leads to

morphological changes, resulting in increased roughness. Consequently, we can conclude that the degradation is morphological in nature. The spectral shift and the appearance of new bands in the EL spectra are due to TCTA aggregation caused by excitons formed after continuous electrical driving or UV irradiation. Impedance spectroscopy studies on single-layer OLEDs showed that the formation of aggregates after UV irradiation affects charge injection and transport in the TCTA layer. UV stress led to the formation of electrically-active defects. The electrically-active behavior of the green (electromer) and red (electroplex) emission bands is consistent with the formation of electrically-active defects upon ageing. Thus, the molecular aggregation of TCTA induced by excitons leads to the formation of trap levels within the TCTA gap, which contribute to the emission of electromer and electroplex.

Contents of Supporting Information

Optical degradation protocol using a UV source; Schematic illustration of the multilayer structure subjected to UV illumination (Figure S1); Electroluminescence (EL) and photoluminescence (PL) spectra of multilayer OLED devices (Figure S2); Comparison of electroluminescence (EL) spectra of fresh-OLEDs with EL and photoluminescence (PL) spectra of stressed-OLEDs (Figure S3); Turn-on voltages and luminances for fresh-OLEDs and stressed-OLEDs (Table S1); Mass spectrum of microcrystalline TCTA powder before and after UV irradiation (Figure S4); ^{1}H NMR spectrum of microcrystalline TCTA powder before UV irradiation (Figure S5); ^{1}H NMR spectrum of microcrystalline TCTA powder after UV irradiation (Figure S6); AFM phase image of TCTA films before and after UV irradiation (Figure S7)

REFERENCES

(1) Tang, C. W.; VanSlyke, S. A. Organic Electroluminescent Diodes. *Appl. Phys. Lett.* **1987**, *51* (12), 913–915. https://doi.org/10.1063/1.98799.

(2) Singh, M.; Jou, J.-H.; Sahoo, S.; SS, S.; He, Z.-K.; Krucaite, G.; Grigalevicius, S.; Wang, C.-W. High Light-Quality OLEDs with a Wet-Processed Single Emissive Layer. *Sci. Rep.* **2018**, *8* (1), 7133. https://doi.org/10.1038/s41598-018-24125-4.

(3) Salehi, A.; Fu, X.; Shin, D.; So, F. Recent Advances in OLED Optical Design. *Adv. Funct. Mater.* **2019**, *29* (15), 1808803. https://doi.org/10.1002/adfm.201808803.

(4) Jou, J.-H.; Sahoo, S.; Dubey, D. K.; Yadav, R. A. K.; Swayamprabha, S. S.; Chavhan, S. D. Molecule-Based Monochromatic and Polychromatic OLEDs with Wet-Process Feasibility. *J. Mater. Chem. C* **2018**, *6* (43), 11492–11518. https://doi.org/10.1039/C8TC04203A.

(5) D'Andrade, B. W.; Forrest, S. R. White Organic Light□Emitting Devices for Solid□State Lighting. *Adv. Mater.* **2004**, *16* (18), 1585–1595. https://doi.org/10.1002/adma.200400684.

(6) Sun, Y.; Giebink, N. C.; Kanno, H.; Ma, B.; Thompson, M. E.; Forrest, S. R. Management of Singlet and Triplet Excitons for Efficient White Orgagenic Light-Emitting Devices. *Nature* **2006**, *440* (7086), 908–912. https://doi.org/10.1038/nature04645.

(7) Sasabe, H.; Kido, J. Development of High Performance OLEDs for General Lighting. *J. Mater. Chem. C* **2013**, *1* (9), 1699–1707. https://doi.org/10.1039/C2TC00584K.

(8) *Flexible & Foldable OLED Displays 2019-2029*; **2018**. https://www.idtechex.com/en/research-report/flexible-and-foldable-oled-displays-2019-2029/629

(9) Tankelevičiūtė, E.; Samuel, I. D. W.; Zysman-Colman, E. The Blue Problem: OLED Stability and Degradation Mechanisms. *J. Phys. Chem. Lett.* **2024**, *15* (4), 1034–1047. https://doi.org/10.1021/acs.jpclett.3c03317.

(10) Tao, Y.; Yang, C.; Qin, J. Organic Host Materials for Phosphorescent Organic Light-Emitting Diodes. *Chem. Soc. Rev.* **2011**, *40* (5), 2943–2970. https://doi.org/10.1039/C0CS00160K.

(11) Xiao, L.; Chen, Z.; Qu, B.; Luo, J.; Kong, S.; Gong, Q.; Kido, J. Recent Progresses on Materials for Electrophosphorescent Organic Light□Emitting Devices. *Adv. Mater.* **2011**, *23* (8), 926–952. https://doi.org/10.1002/adma.201003128.

(12) Masui, K.; Nakanotani, H.; Adachi, C. Analysis of Exciton Annihilation in High-Efficiency Sky-Blue Organic Light-Emitting Diodes with Thermally Activated Delayed Fluorescence. *Org. Electron.* **2013**, *14* (11), 2721–2726. https://doi.org/10.1016/j.orgel.2013.07.010.

(13) Ho, C.-L.; Chi, L.-C.; Hung, W.-Y.; Chen, W.-J.; Lin, Y.-C.; Wu, H.; Mondal, E.; Zhou, G.-J.; Wong, K.-T.; Wong, W.-Y. Carbazole-Based Coplanar Molecule (CmInF) as a Universal Host for Multi-Color Electrophosphorescent Devices. *J. Mater. Chem.* **2012**, *22* (1), 215–224. https://doi.org/10.1039/C1JM13794H.

(14) Li, J.; Ding, D.; Tao, Y.; Wei, Y.; Chen, R.; Xie, L.; Huang, W.; Xu, H. A Significantly Twisted Spirocyclic Phosphine Oxide as a Universal Host for High□Efficiency Full□Color Thermally Activated Delayed Fluorescence Diodes. *Adv. Mater.* **2016**, *28* (16), 3122–3130. https://doi.org/10.1002/adma.201506286.

(15) Li, W.; Li, J.; Wang, F.; Gao, Z.; Zhang, S. Universal Host Materials for High-Efficiency Phosphorescent and Delayed-Fluorescence OLEDs. *ACS Appl. Mater. Interfaces* **2015**, *7* (47), 26206–26216. https://doi.org/10.1021/acsami.5b08291.

(16) Yersin, H. *Highly Efficient OLEDs with Phosphorescent Materials*; John Wiley & Sons, 2008.

(17) Helander, M. G.; Wang, Z. B.; Qiu, J.; Greiner, M. T.; Puzzo, D. P.; Liu, Z. W.; Lu, Z. H. Chlorinated Indium Tin Oxide Electrodes with High Work Function for Organic Device Compatibility. *Science* **2011**, *332* (6032), 944–947. https://doi.org/10.1126/science.1202992.

(18) Wang, Z. B.; Helander, M. G.; Qiu, J.; Puzzo, D. P.; Greiner, M. T.; Hudson, Z. M.; Wang, S.; Liu, Z. W.; Lu, Z. H. Unlocking the Full Potential of Organic Light-Emitting Diodes on Flexible Plastic. *Nat. Photonics* **2011**, *5* (12), 753–757. https://doi.org/10.1038/nphoton.2011.259.

(19) Xia, S. C.; Kwong, R. C.; Adamovich, V. I.; Weaver, M. S.; Brown, J. J. OLED Device Operational Lifetime: Insights and Challenges. In *2007 IEEE International Reliability Physics Symposium Proceedings. 45th Annual*; IEEE, 2007; pp 253–257. https://doi.org/10.1109/RELPHY.2007.369901.

(20) Brunner, K.; Van Dijken, A.; Börner, H.; Bastiaansen, J. J. A. M.; Kiggen, N. M. M.; Langeveld, B. M. W. Carbazole Compounds as Host Materials for Triplet Emitters in Organic Light-Emitting Diodes: Tuning the HOMO Level without Influencing the Triplet Energy in Small Molecules. *J. Am. Chem. Soc.* **2004**, *126* (19), 6035–6042. https://doi.org/10.1021/ja049883a.

(21) Ambrose, J. F.; Nelson, R. F. Anodic Oxidation Pathways of Carbazoles: I. Carbazole and N-Substituted Derivatives. *J. Electrochem. Soc.* **1968**, *115* (11), 1159. https://doi.org/10.1149/1.2410929.

(22) Scholz, S.; Walzer, K.; Leo, K. Analysis of Complete Organic Semiconductor Devices by Laser Desorption/Ionization Time□of□Flight Mass Spectrometry. *Adv. Funct. Mater.* **2008**, *18* (17), 2541–2547. https://doi.org/10.1002/adfm.200700816.

(23) Wang, Q.; Sun, B.; Aziz, H. Exciton–Polaron-Induced Aggregation of Wide-Bandgap Materials and Its Implication on the Electroluminescence Stability of Phosphorescent Organic Light-Emitting Devices. *Adv. Funct. Mater.* **2014**, *24* (20), 2975–2985. https://doi.org/10.1002/adfm.201303840.

(24) Yu, H.; Zhang, Y.; Cho, Y. J.; Aziz, H. Exciton-Induced Degradation of Carbazole-Based Host Materials and Its Role in the Electroluminescence Spectral Changes in Phosphorescent Organic Light Emitting Devices with Electrical Aging. *ACS Appl. Mater. Interfaces* **2017**, *9* (16), 14145–14152. https://doi.org/10.1021/acsami.7b01432.

(25) Kalinowski, J.; Giro, G.; Cocchi, M.; Fattori, V.; Di Marco, P. Unusual Disparity in Electroluminescence and Photoluminescence Spectra of Vacuum-Evaporated Films of 1,1-Bis ((Di-4-Tolylamino) Phenyl) Cyclohexane. *Appl. Phys. Lett.* **2000**, *76* (17), 2352–2354. https://doi.org/10.1063/1.126343.

(26) Birks, J. B. Excimers. *Rep. Prog. Phys.* **1975**, *38* (8), 903. https://doi.org/10.1088/0034-4885/38/8/001.

(27) Granlund, T.; Pettersson, L. A.; Anderson, M. R.; Inganäs, O. Interference Phenomenon Determines the Color in an Organic Light Emitting Diode. *J. Appl. Phys.* **1997**, *81* (12), 8097–8104. https://doi.org/10.1063/1.365418.

(28) Park, Y.; Lee, S.; Kim, K.; Kim, S.; Lee, J.; Kim, J. Exciplex□Forming Co□host for Organic Light□Emitting Diodes with Ultimate Efficiency. *Adv. Funct. Mater.* **2013**, *23* (39), 4914–4920. https://doi.org/10.1002/adfm.201300547.

(29) Yang, S.; Jiang, M. White Light Generation Combining Emissions from Exciplex, Excimer and Electromer in TAPC-Based Organic Light-Emitting Diodes. *Chem. Phys. Lett.* **2009**, *484* (1–3), 54–58. https://doi.org/10.1016/j.cplett.2009.11.005.

(30) Lin, Y.-T.; Chen, L.-Y.; Wu, C.-C.; Wong, K.-T.; Chen, R.-T.; Chien, Y.-Y. Influences of Device Architectures on Characteristics of Organic Light-Emitting Devices Incorporating Ambipolar Blue-Emitting Ter (9, 9-Diarylfluorenes). *Int. J. Opt. Photonics* **2008**, *2* (1), 45–58.

(31) Miśnik, M.; Falkowski, K.; Mróz, W.; Stampor, W. Electromodulation of Photoluminescence in Vacuum-Evaporated Films of Bathocuproine. *Chem. Phys.* **2013**, *410*, 45–54. https://doi.org/10.1016/j.chemphys.2012.10.013.

(32) El Housseiny, H.; Mbarki, G.; Buso, D.; Ternisien, M.; Zissis, G.; Renaud, C. Exciplex-Based Organic Light-Emitting Diodes with Deep Blue Emission. In *Organic Electronics and Photonics: Fundamentals and Devices IV*; SPIE, 2024; Vol. 13013, pp 9–17. https://doi.org/10.1117/12.3022876.

(33) Kondakov, D. Y.; Lenhart, W. C.; Nichols, W. F. Operational Degradation of Organic Light-Emitting Diodes: Mechanism and Identification of Chemical Products. *J. Appl. Phys.* **2007**, *101* (2), 024512. https://doi.org/10.1063/1.2430922.

(34) Lu, M.-H.; Madigan, C. F.; Sturm, J. C. Improved External Coupling Efficiency in Organic Light-Emitting Devices on High-Index Substrates. In *International Electron Devices Meeting 2000. Technical Digest. IEDM (Cat. No. 00CH37138)*; IEEE, 2000; pp 607–610. https://doi.org/10.1109/IEDM.2000.904393.

(35) Deng, Y.; Keum, C.; Hillebrandt, S.; Murawski, C.; Gather, M. C. Improving the Thermal Stability of Top-Emitting Organic Light-Emitting Diodes by Modification of the Anode

Interface. *Adv. Opt. Mater.* **2021**, *9* (14), 2001642. https://doi.org/10.1002/adom.202001642.

(36) Blondel, B.; Colin, A.; Lopes, M.; Alary, F.; Zissis, G.; Sasaki, I.; Renaud, C. Application of [Pt (II)(Tetra-Tert-Butylsalophen)] Complex within Organic Devices: Deep Red Emission, Bistable Light-Emitting Diodes and Operational Stability. *Appl. Sci.* **2018**, *8* (5), 762. https://doi.org/10.3390/app8050762.

(37) Pekkola, O.; Gassmann, A.; Etzold, F.; Laquai, F.; von Seggern, H. Influence of Triplet Excitons on the Lifetime of Polymer-Based Organic Light Emitting Diodes. *Phys. Status Solidi A* **2014**, *211* (9), 2035–2039. https://doi.org/10.1002/pssa.201330411.

(38) Arif, M.; Yun, M.; Gangopadhyay, S.; Ghosh, K.; Fadiga, L.; Galbrecht, F.; Scherf, U.; Guha, S. Polyfluorene as a Model System for Space-Charge-Limited Conduction. *Phys. Rev. B* **2007**, *75* (19), 195202. https://doi.org/10.1103/PhysRevB.75.195202.

(39) Renaud, C.; Nguyen, T.-P. Study of Trap States in Polyspirobifluorene Based Devices: Influence of Aging by Electrical Stress. *J. Appl. Phys.* **2009**, *106* (5), 053707. https://doi.org/10.1063/1.3195086.

(40) Shen, J.; Wang, D.; Langlois, E.; Barrow, W. A.; Green, P. J.; Tang, C. W.; Shi, J. Degradation Mechanisms in Organic Light Emitting Diodes. *Synth. Met.* **2000**, *111*, 233–236. https://doi.org/10.1016/S0379-6779(99)00370-7.

(41) Lee, S.-S. Effect of the Equivalent Resistance of an Organic Light-Emitting Diode (OLED) on the Half-Life during Operation. *J. Korean Phys. Soc.* **2008**, *53* (2), 835–839. https://doi.org/10.3938/jkps.53.835.

(42) Scholz, S.; Kondakov, D.; Lüssem, B.; Leo, K. Degradation Mechanisms and Reactions in Organic Light-Emitting Devices. *Chem. Rev.* **2015**, *115* (16), 8449–8503. https://doi.org/10.1021/cr400704v.

(43) Song, W.; Lee, J. Y. Degradation Mechanism and Lifetime Improvement Strategy for Blue Phosphorescent Organic Light-Emitting Diodes. *Adv. Opt. Mater.* **2017**, *5* (9), 1600901. https://doi.org/10.1002/adom.201600901.

(44) Ban, X.; Sun, K.; Sun, Y.; Huang, B.; Jiang, W. Design of High Triplet Energy Electron Transporting Material for Exciplex-Type Host: Efficient Blue and White Phosphorescent OLEDs Based on Solution Processing. *Org. Electron.* **2016**, *33*, 9–14. https://doi.org/10.1016/j.orgel.2016.02.041.

(45) Liu, M.; Liu, Y.; Peng, Z.; Yang, C.; Mu, Q.; Cao, Z.; Ma, J.; Xuan, L. Controlling Morphology and Aggregation in Semiconducting Polymers: The Role of Solvents on Lasing Emission in Poly [2-Methoxy-5-(2′-Ethyl-Hexyloxy)-1, 4-Phenylene-Vinylene]. *Materials* **2017**, *10* (7), 706. https://doi.org/10.3390/ma10070706.

(46) Li, W.; Zhao, J.; Kong, X.; Du, X.; Li, X.; Zheng, C.; Tao, S. Improving the Performance of Solution-Processed Small Molecule OLEDs via Micro-Aggregation Formed by an Alcohol Additive Incorporation. *Org. Electron.* **2019**, *64*, 252–258. https://doi.org/10.1016/j.orgel.2018.10.039.

(47) Wang, X.; Wang, R.; Zhou, D.; Yu, J. Study of Organic Light-Emitting Diodes with Exciplex and Non-Exciplex Forming Interfaces Consisting of an Ultrathin Rubrene Layer. *Synth. Met.* **2016**, *214*, 50–55. https://doi.org/10.1016/j.synthmet.2016.01.022.

(48) Ivaniuk, K.; Cherpak, V.; Stakhira, P.; Baryshnikov, G.; Minaev, B.; Hotra, Z.; Turyk, P.; Zhydachevskii, Y.; Volyniuk, D.; Aksimentyeva, O. BaZrO3 Perovskite Nanoparticles as

Emissive Material for Organic/Inorganic Hybrid Light-Emitting Diodes. *Dyes Pigments* **2017**, *145*, 399–403. https://doi.org/10.1016/j.dyepig.2017.06.020.

(49) Lu, H.-W.; Weng, H.-L.; Kao, P.-C.; Chu, S.-Y.; Juang, Y.-D. Fabrication of Color-Tunable Blue-Violet Organic Light Emitting Diodes for White Light Source. *ECS J. Solid State Sci. Technol.* **2016**, *5* (6), R104. https://doi.org/10.1149/2.0151606jss.

(50) Wei, M.; Gui, G.; Chung, Y.-H.; Xiao, L.; Qu, B.; Chen, Z. Micromechanism of Electroplex Formation. *Phys. Status Solidi B* **2015**, *252* (8), 1711–1716. https://doi.org/10.1002/pssb.201552098.

(51) Zhang, J.; Chen, Z.; Liu, Y.; Huang, M.; Wei, Q.; Gong, Q. Improvement on the Photorefractive Performance of a Monolithic Molecular Material by Introducing Electron Traps. *Appl. Phys. Lett.* **2004**, *85* (8), 1323–1325. https://doi.org/10.1063/1.1784522.

(52) Kondakov, D. Y. Role of Chemical Reactions of Arylamine Hole Transport Materials in Operational Degradation of Organic Light-Emitting Diodes. *J. Appl. Phys.* **2008**, *104* (8), 084520. https://doi.org/10.1063/1.3006890.

(53) Nowy, S.; Ren, W.; Elschner, A.; Lövenich, W.; Brütting, W. Impedance Spectroscopy as a Probe for the Degradation of Organic Light-Emitting Diodes. *J. Appl. Phys.* **2010**, *107* (5). https://doi.org/10.1063/1.3294642.

(54) Altazin, S.; Züfle, S.; Knapp, E.; Kirsch, C.; Schmidt, T. D.; Jäger, L.; Noguchi, Y.; Brütting, W.; Ruhstaller, B. Simulation of OLEDs with a Polar Electron Transport Layer. *Org. Electron.* **2016**, *39*, 244–249. https://doi.org/10.1016/j.orgel.2016.10.014.

(55) Brütting, W.; Berleb, S.; Mückl, A. G. Device Physics of Organic Light-Emitting Diodes Based on Molecular Materials. *Org. Electron.* **2001**, *2* (1), 1–36. https://doi.org/10.1016/S1566-1199(01)00009-X.

(56) Kondakov, D. Y.; Sandifer, J. R.; Tang, C. W.; Young, R. H. Nonradiative Recombination Centers and Electrical Aging of Organic Light-Emitting Diodes: Direct Connection between Accumulation of Trapped Charge and Luminance Loss. *J. Appl. Phys.* **2003**, *93* (2), 1108–1119. https://doi.org/10.1063/1.1531231.

(57) Nowy, S.; Ren, W.; Wagner, J.; Weber, J. A.; Brütting, W. Impedance Spectroscopy of Organic Hetero-Layer OLEDs as a Probe for Charge Carrier Injection and Device Degradation. In *Organic Light Emitting Materials and Devices XIII*; SPIE, 2009; Vol. 7415, pp 79–90. https://doi.org/10.1117/12.824856.

(58) Luo, Y.; Aziz, H.; Xu, G.; Popovic, Z. D. Improving the Stability of Organic Light-Emitting Devices by Using a Hole-Injection-Tunable-Anode-Buffer-Layer. *J. Appl. Phys.* **2007**, *101* (5). https://doi.org/10.1063/1.2472254.

(59) Buso, D.; Bhosle, S.; Liu, Y.; Ternisien, M.; Renaud, C.; Chen, Y. OLED Electrical Equivalent Device for Driver Topology Design. *IEEE Trans. Ind. Appl.* **2013**, *50* (2), 1459–1468. https://doi.org/10.1109/TIA.2013.2272432.

(60) Cho, Y. J.; Taylor, S.; Aziz, H. Increased Electromer Formation and Charge Trapping in Solution-Processed versus Vacuum-Deposited Small Molecule Host Materials of Organic Light-Emitting Devices. *ACS Appl. Mater. Interfaces* **2017**, *9* (46), 40564–40572. https://doi.org/10.1021/acsami.7b15190.

(61) Kwon, S.; Wee, K.-R.; Pac, C.; Kang, S. O. Significance of Irreversible Formation of "Electromer" in 1-Bis[4-[N,N-Di(4-Tolyl)Amino]Phenyl]-Cyclohexane Layer Associated with the Stability of Deep Blue Phosphorescent Organic Light Emitting Diodes. *Org. Electron.* **2012**, *13* (4), 645–651. https://doi.org/10.1016/j.orgel.2011.12.022.

(62) Kalinowski, J.; Cocchi, M.; Di Marco, P.; Stampor, W.; Giro, G.; Fattori, V. Impact of High Electric Fields on the Charge Recombination Process in Organic Light-Emitting Diodes. *J. Phys. Appl. Phys.* **2000**, *33* (19), 2379. https://doi.org/10.1088/0022-3727/33/19/306.

(63) Liu, X.-K.; Chen, Z.; Zheng, C.-J.; Liu, C.-L.; Lee, C.-S.; Li, F.; Ou, X.-M.; Zhang, X.-H. Prediction and Design of Efficient Exciplex Emitters for High-Efficiency, Thermally Activated Delayed-Fluorescence Organic Light-Emitting Diodes. *Adv. Mater.* **2015**, *27* (14), 2378–2383. https://doi.org/10.1002/adma.201405062.

(64) Zhang, F.; Zhao, S.; Zhao, D.; Jiang, W.; Li, Y.; Yuan, G.; Zhu, H.; Xu, Z. Electroplex Emission from Bi-Layer Blue Emitting Organic Materials. *Phys. Scr.* **2007**, *75* (4), 407. https://doi.org/10.1088/0031-8949/75/4/004.

(65) Al Attar, H. A.; Monkman, A. P. Electric Field Induce Blue Shift and Intensity Enhancement in 2D Exciplex Organic Light Emitting Diodes; Controlling Electron–Hole Separation. *Adv. Mater.* **2016**, *28* (36), 8014–8020. https://doi.org/10.1002/adma.201600965.

(66) Kalinowski, J.; Cocchi, M.; Virgili, D.; Fattori, V.; Williams, J. A. G. Evidence for Electric Field Dependent Dissociation of Exciplexes in Electron Donor–Acceptor Organic Solid Films. *Chem. Phys. Lett.* **2006**, *432* (1–3), 110–115. https://doi.org/10.1016/j.cplett.2006.10.059.

(67) Kalinowski, J.; Giro, G.; Cocchi, M.; Fattori, V.; Zamboni, R. The Nature of Emitting States in Electroluminescence of Polymeric Films Doped with Anthracene and Anthracene-Based Supramolecules. *Chem. Phys.* **2002**, *277* (3), 387–396. https://doi.org/10.1016/S0301-0104(02)00333-6.

(68) Yoshida, H.; Yoshizaki, K. Electron Affinities of Organic Materials Used for Organic Light-Emitting Diodes: A Low-Energy Inverse Photoemission Study. *Org. Electron.* **2015**, *20*, 24–30. https://doi.org/10.1016/j.orgel.2015.01.037.

(69) Renaud, C.; Nguyen, T.-P. Identification of the Nature of Trapping Centers in Polyspirobifluorene Based Diodes by Using Electrical Characterization. *J. Appl. Phys.* **2010**, *107* (12), 124505. https://doi.org/10.1063/1.3428962.